Mechanoresponsive Alignment of Molecular Self-assembled Negatively Charged Nanofibrils

Shijin Zhang[1,†], William Cortes[1,†], Toshio Sasaki[2], Shunsuke Asahina[3], Asano Natsuko[3], Qizheng Zhang[1], Ye Zhang[1,]*

[1]Bioinspired Soft Matter Unit, Okinawa Institute of Science and Technology Graduate University, 1919-1 Tancha, Onna-son, Okinawa 904-0495 Japan

[2]Imaging Section, Okinawa Institute of Science and Technology Graduate University, 1919-1 Tancha, Onna-son, Okinawa 904-0495, Japan

[3]SM Application Group, JEOL Ltd., Akishima, Tokyo 196-8558, Japan

†Those authors contribute equally to the work.

KEYWORDS: Taurine; hierarchical assembly; nanofibril alignment; mechano-responsive; birefringence; lamellar domain.

ABSTRACT: Inspired by the mechanoresponsive orientation of actin filaments in cell, we introduce a design paradigm of synthetic molecular self-assembling fibrils that respond to external mechanical force by transforming from a macroscopically disorder state to a highly ordered uniaxial aligned state. The incorporation of aromatic-containing amino acids and negatively charged amino acids lead to self-assembly motifs that transform into uniform nanofibrils in acidic solution. Adjusting the pH level of aqueous solution introduces optimal negative charge to the

surface of self-assembling nanofibrils inducing long-range electrostatic repulsion forming a nematic phase. Upon external mechanical force, nanofibrils align in the force direction. Via evaporation casting in capillary confinement, the solvated synthetic self-assembling nanofibrils transform into scalable lamellar domains. Adjusting capillary geometry and drying procedure offers further parameters for tuning the mesoscale alignment of nanofibrils generating a variety of interference colors. The design paradigm of mechanoresponsive alignment of self-assembled nanofibrils as an addition of nanofabrication techniques is potentially employable for realizing biomimetic optical structures.

INTRODUCTION

Under physiological conditions, monomeric G-actin proteins self-assemble into long, and moderately flexible actin filaments that tend to spontaneously align to form liquid crystal (LC).[1] Upon application of optimal mechanical forces to a cell, actin filaments self-organize collectively with respect to both position and orientation in the cytoplasm, which determines the cellular shape and motility. Creating such mechano-responsive active filaments via synthetic chemistry is one of the ultimate goals of biomimetic materials research. For a given polymer-based filamentary network, there exist numerous, potentially industrially-scalable techniques to control micro- or nano-fibril alignment towards functional materials by mechanical force.[2,3] However, investigations of molecular-self-assembly-constructed filaments' responsiveness to mechanical forces applied macroscopically are rarely reported.[4,5] In contrast to polymer-based filaments, in which ordering is driven by interfilament interactions, molecular-self-assembly-constructed filaments form lyotropic phases stabilized by not only interfilament interactions but also intermolecular interactions that lend themselves to diverse morphologies, necessary to realizing the most pertinent applications of self-assemblies,[6] but likewise impeding the long-range order over scales appreciable to these uses.[7]

Therefore, hierarchical regulation[5, 8-10] is critical to the macroscopic control of the alignment of molecular self-assembly systems responding to mechanical force.

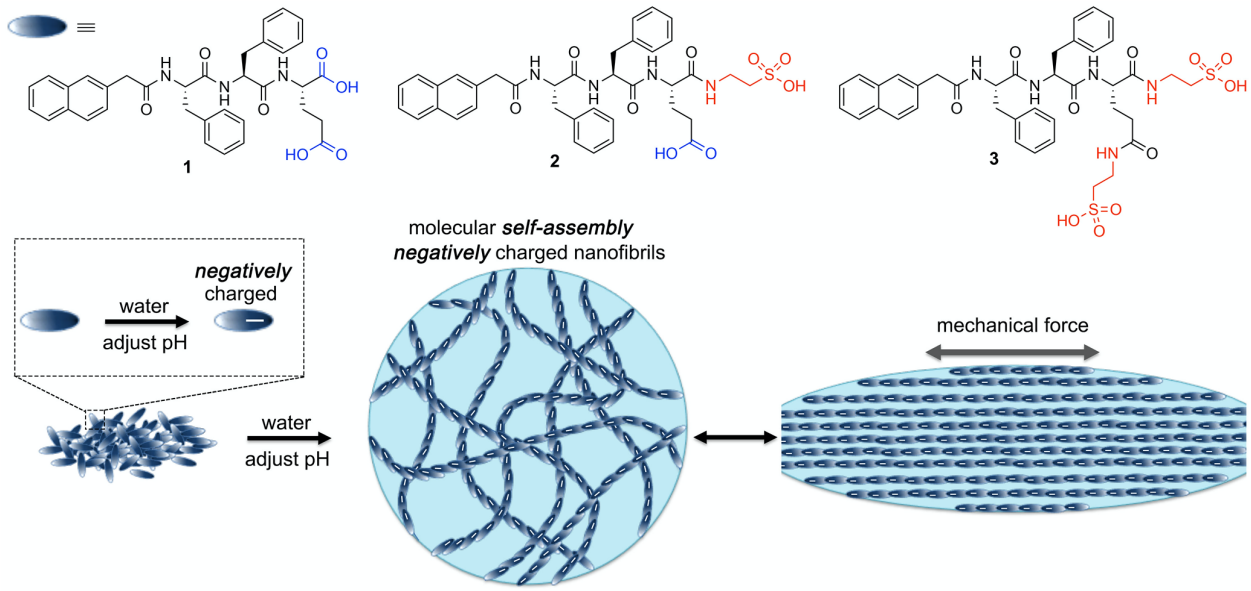

Figure 1. Chemical structures of designed molecules for self-assembled filaments carrying negative charge, and schematic illustration of mechano-responsive alignment of self-assembled nanofibrils.

Regarding the biomimetic capabilities of small molecular self-assembly peptides,[11, 12] we suggest a design paradigm for a hierarchically controllable artificial system that responds to mechanical force for higher order alignment. As shown in Figure 1, naphthalene-phenylalanine-phenylalanine (NapFF) serves as an essential motif for π-π interaction and hydrogen bonding oriented molecular self-assembly.[13] Inspired by the spontaneous long-range ordering of negatively charged actin filaments due to the existence of a long-range anisotropic electrostatic interaction that torques neighboring filaments into alignment with each other,[14] we incorporate glutamic acid in the C-terminus of NapFF to obtain molecule **1** having two protonatable functional groups, α-COOH and φ-COOH. Due to its high acid dissociation relative to other amino acids, taurine was incorporated

to the α-COOH or to both -COOH groups of **1** leading to molecule **2** and **3**, respectively. All three molecules bear anisotropic electron distributions. By altering the pH level of aqueous solutions, molecules **1**, **2** and **3** exhibit various charge states introducing tunable electrostatic repulsion between molecules. Such electrostatic interactions, together with π-π interaction and hydrogen bonding, guide molecular self-assembly of the three molecules. The obtained self-assembling nanofilaments inherit the negative charges facilitating uniaxial orientation upon mechanical force for higher order organization (Figure 1).

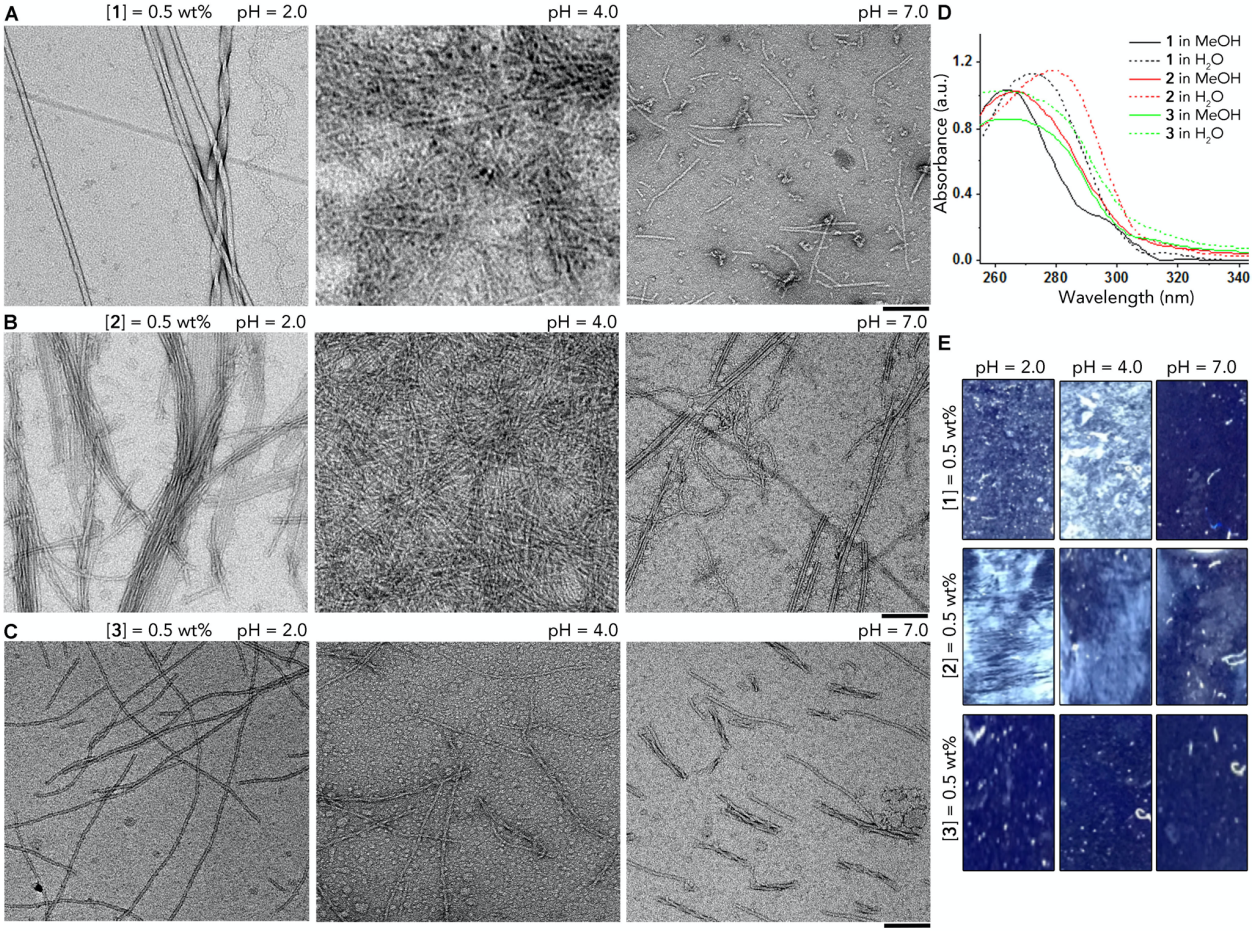

Figure 2. TEM images of nano-filaments formed by self-assembly of molecule **1** (A), **2** (B), or **3** (C) in water (0.5 wt%) at pH 2.0, 4.0, and 7.0. Scale bars represent 100 nm. (D) UV-vis absorption of molecules **1**, **2**, and **3** in MeOH (solid lines) *vs*. in water (dash lines) at the same concentration

(0.5 wt%). (E) Optical birefringence of molecules **1**, **2**, and **3** in water (0.5 wt%) at pH 2.0, 4.0, and 7.0. The solutions are contained in a standard 1 mm quartz cuvette, viewed between perpendicularly crossed polarizers (Figure S1).

Based on the pKa values of α-COOH and φ-COOH of L-glutamic acid, and -SO_3H of taurine, which are 2.10, 4.07, and 1.5,[15] respectively, we adjusted the solutions of molecules **1**, **2** and **3** to three pH levels, 2.0, 4.0 and 7.0 to obtain a variety of negative charge states (Table S1). At pH 2.0, molecules **1**, **2** and **3** bear 0.45, 0.77, and 1.52 negative charges, respectively. At pH 4.0, they carry 1.43, 1.44, and 1.99 negative charges, respectively. At pH 7.0, all three molecules bear 2.0 negative charges. Considering the fact that the charge state of a molecule governs its conformation with implications for molecular self-assembly,[16] we use transmission electron microscopy (TEM) to characterize the morphology of self-assembly of the three molecules at different pH levels.

As shown in Figure 2A, self-assembly of molecule **1** (Figure 2A) forms both 13 nm wide nanofibrils and 21 nm wide twisted nanoribbons at pH 2.0. At pH 4.0, uniform nanofibrils with a width of 8 nm are formed, while at pH 7.0, short nanostrands with 8 nm width are observed. In Figure 2B, molecule **2** self-assembles into paracrystalline bundles of aligned nanofibrils with an average width of 8 nm at pH 2.0, disordered nanofibrils with the same width 8 nm but much higher density at pH 4.0, and a mixture of nanofibrils (8 nm width) and nanotubes (10 nm width) at pH 7.0. In Figure 2C, molecule **3** self-assembles into nanofibrils of the same width (8 nm) as those of molecule **2** but at very low density at pH 2.0. By increasing the pH level, shorter nanostrands with the same width are formed at pH 4.0 and 7.0. Since fibrous structure is essential to long-rang mechanotransduction and mechanosensing,[17] self-assembly of molecule **1** at pH 4.0, and self-assembly of molecule **2** at pH 2.0 or 4.0 possess the optimal morphology to potentially respond to external mechanical force.

Comparing the UV-vis absorption of molecular self-assembly in water with monodispersed molecules in methanol at the same concentration (Figure 2D), we found that both molecule **1** and **2** exhibited clear redshifts at self-assembling states. Such J-aggregation[18] correlated absorption suggests a nematic-like slipped stacking of molecule within its aromatic domains.[19] Consistent to their absorption spectra, both molecules **1** and **2** show birefringence at self-assembling states of nanofibrous structures. Specifically, self-assembly of molecule **1** shows birefringence at both pH 2.0 and 4.0 accompanied with sol-gel transitions (Figure S2) suggesting spatial nanofibril alignment induced by poor mobility.[20, 21] While self-assembly of molecule **2** shows obvious birefringence at pH 2.0 and 4.0 without forming stabilized hydrogel. By increasing the pH level, the birefringence intensity decreases. The characterizations suggest that high-density nanofibrils, formed by a nematic-like slipped stacking of molecules bearing negative charge between 0.77 and 1.44, exhibit an orientation induced strong birefringence.

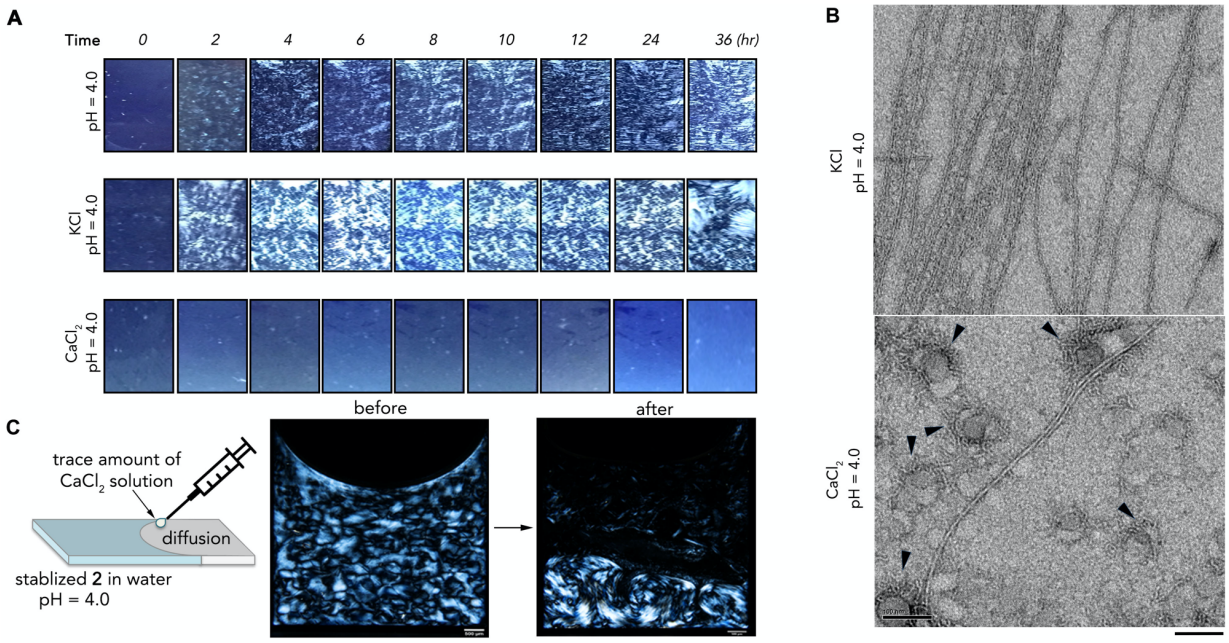

Figure 3. (A) Time-dependent optical birefringence images of molecule **2** (0.5 wt%) in water, in KCl (20 mM) solution, and $CaCl_2$ (10mM) solution at pH 4.0. (B) TEM images of molecule **2** (0.5

wt%) in KCl (20 mM) solution, and $CaCl_2$ (10mM) solution at pH 4.0. Scale bar represents 100 nm. (C) Schematic illustration of the introduction of trace amounts $CaCl_2$ solution (pH 4.0) to the surface of self-assembled molecule **2** (0.5 wt%) in water at pH 4.0 (left); optical birefringence images of molecule **2** (0.5 wt%) in water at pH 4.0 before and after the addition of trace amount $CaCl_2$ solution (right).

Therefore, we selected self-assembly of **2** at pH 4.0 exhibiting moderate birefringence and fluidity to study the influence of electrostatic interaction on molecular self-assembly. We monitored the birefringence from the beginning of self-assembly in real-time through perpendicularly crossed polarizers for 36 hours by adding salts of K^+, and Ca^{2+} into the solution of **2** before the initiation of self-assembly (Figure 3A). Compared to the steady enhancement of birefringence following the progress of molecular self-assembly, the addition of monovalent cation K^+ did not interrupt the steady growth of birefringence, while the addition of divalent ion Ca^{2+} repressed the generation of birefringence. TEM images exhibited uniform nanofibrils with 8 nm width upon the addition of KCl confirming the undisturbed self-assembly process (Figure 3B upper panel). Upon incubation with $CaCl_2$, self-assembly of **2** formed aggregates of short nanostrands mixed with few nanofibrils confirming a disrupted self-assembly process. Since molecule **2** bears 1.44 negative charge at pH 4.0, divalent cations may behave as ion bridges[22] affecting the intermolecular interactions and inducing aggregation. By adding $CaCl_2$ to a stabilized self-assembly of **2** in a confined container, we introduced the territorial binding of counterions into nanofibers bearing negative charges (Figure 3C). Before the addition of $CaCl_2$, the stabilized birefringence indicates the formation of spatially ordered nanofibrils. Following the diffusion of Ca^{2+} into the solution of **2**, birefringence vanished. TEM images confirmed the transition from

nanofibrils into nanoaggregates (Figure S5) indicating that electrostatic interaction is critical to spatial orientation of molecular self-assembled nanofibrils.

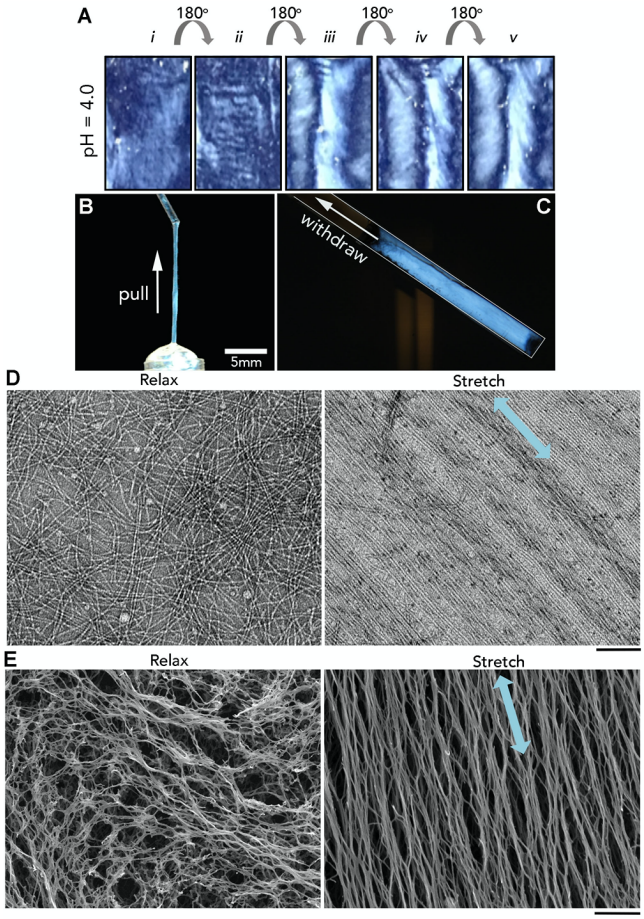

Figure 4. (A) Optical birefringence images of stabilized self-assembly of molecule **2** (0.5 wt%) in aqueous solution at pH 4.0 going through sequential vertical rotations. Optical birefringence images of stabilized self-assembly of molecule **2** (0.5 wt%) in aqueous solution at pH 4.0 pulled using a glass pipette (B) and withdrawn into round quartz capillary with a diameter of 1 mm (C). (D) TEM images of self-assembly of molecule 2 (0.5 wt%) in aqueous solution at pH 4.0 at relaxed state (left) and under stretching force (right). The blue arrow indicates the stretch axis. The scale bar represents 100 nm. (E) SEM images of stabilized self-assembly of molecule **2** (0.5 wt%) in aqueous solution at pH 4.0 at relaxed state (left) and under stretching force (right). The blue arrow indicates the stretch axis. The scale bar represents 20 μm.

To examine the mechano-response of molecular self-assembly of **2** bearing negative charge at pH 4.0, a sealed cuvette filled with solution of **2** exhibiting stabilized birefringence was rotated vertically. After two rounds of rotations, the intensity of birefringence was dramatically enhanced indicating high order spatial alignment of nanofibrils (Figure 4A). Further rotation did not affect the birefringence intensity nor disrupt the birefringence pattern suggesting a relatively stable fiber alignment under the same mechanical force. By pulling the solution of **2** with a glass pipette (Figure 4B) or drawing the solution into a quartz capillary (Figure 4C), we observed enhanced birefringence through the cross polarizer suggesting a stretch force or shear force induced nanofibril alignment, respectively. TEM images showed disordered nanofibrils tangled with each other in a relaxed state, and parallelly aligned nanofibrils along the external force axis upon stretching (Figure 4D). Scanning electron microscopy (SEM) images exhibited the same mechanoresponsive behavior of nanofibrous bundles (Figure 4E). Consistent to their birefringence, self-assembled nanofibrils of **2** respond to mechanical force achieving higher order alignment in the force direction.

The regulation of hierarchical assemblies in a scalable manner[23-25] is a critical challenge in bottom-up materials synthesis.[26] Following the invention of fabrication of uniformly oriented cellulose nanocrystal film in capillary confinement,[27] we intend to scale up the fabrication of highly ordered nanostructured peptide film under confined drying conditions within thin capillaries. As indicated in Figure 5A, a thin-walled rectangular capillary (50 μm height, width 1 mm) is filled with solvated self-assembly of **2** via wetting-induced upward flow. The slow evaporation at the top meniscus by the presence of the saturated vapor, combined with fast water evaporation at the bottom, causes asymmetric drying of the self-assembled nanofibrils and flow to the pinned interface right after

pulling the capillary out. After transferring the capillary to a horizontal position, we monitored the orientation transition of nanofibrils in real-time using polarized optical microscopy (POM).

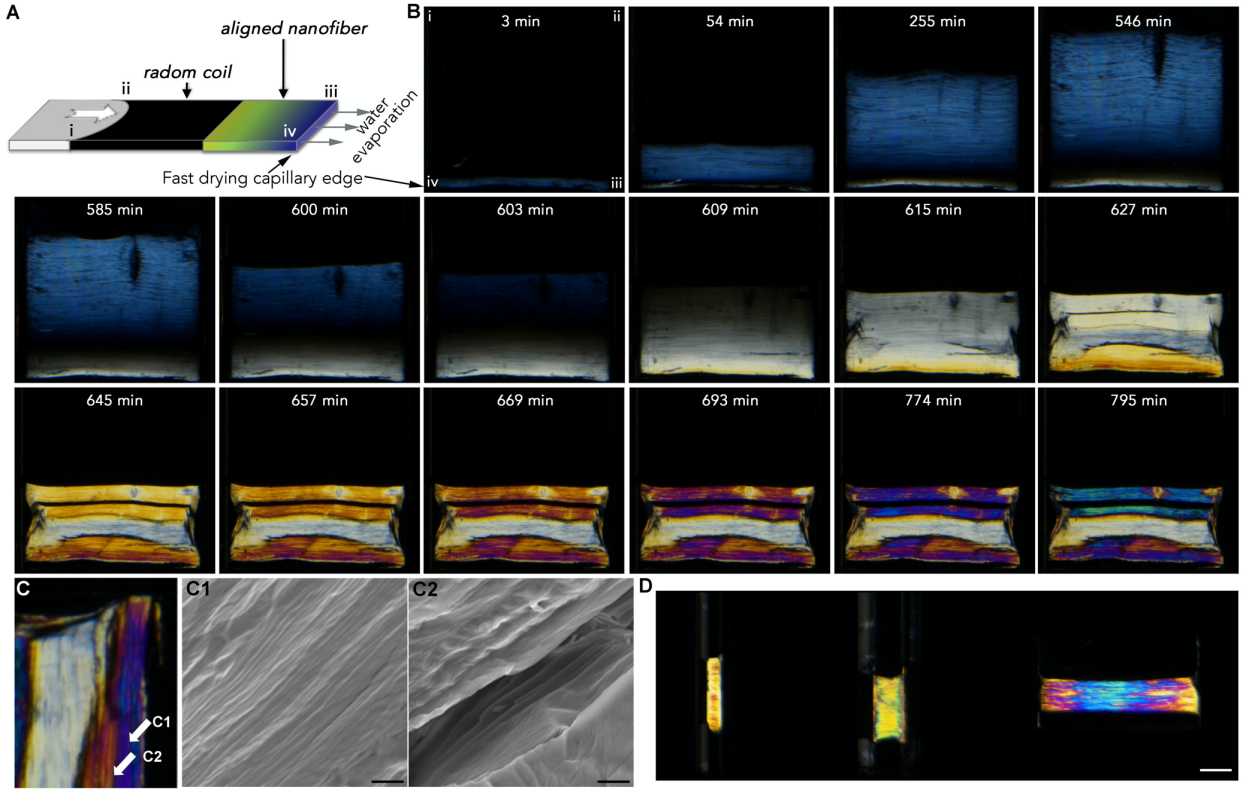

Figure 5. (A) Schematic diagram of evaporation casting in a rectangular capillary. (i-iv) indicate capillary orientation in subsequent sub-figures. (B) Polarized optical microscopy (POM) time-lapse of evaporation casting of molecule **2** (0.5 wt%) in pure water at pH 4.0 in rectangular capillary (50 μm height, width 1 mm). (C) Zoomed in POM image of the last image in panel B with two indicated positions for SEM imaging. C1 represents the surface of the evaporation-induced film. C2 is SEM image of wall-to-wall crack parallel to the drying edge. Scale bars in panel C1 and C2 represent 1 μm, and scale bar in panel C3 represents 100 nm. (D) POM images of evaporation casting of molecule **2** (0.5 wt%) in pure water at pH 4.0 under varying capillary dimensions. From left to right, the dimension of the capillary is 0.05 x 0.05 mm, 0.1 x 0.1 mm,

and 0.05 x 0.5 mm. Images were selected from times when qualitative changes in birefringent domains were no longer observed. Scale bar represents 100 μm.

As shown in Figure 5B, in a micro-capillary environment, flow driven by differential evaporation rates induced alignment of self-assembling nanofibrils into uniform highly-ordered birefringent lamellar domains. Within the first 9 hours of evaporation, the expansion of birefringent area to the opposite direction of the flow suggests a condensation of nanofibrils. Following the shrinkage of birefringent area, the solidification of uniformly oriented nanofibrils along the drying capillary edge was accelerated exhibiting white interference color. Once the solidification was almost complete after 10 hours of evaporation, the close stacking of nanofibrils is initiated, and vertical cracks parallel to the drying edge of the capillary are formed due to the mismatch of morphology between the twisted structures and the rectangular capillary walls, which divides the lamellar domains into 4 sections. At the late drying stage, the shrinkage of the lamellar domains induces interference color shifting up in wavelength from white to yellow, orange, purple, blue or green, correlated to close stacking of highly ordered nanofibrils.

SEM images of the evaporation-induced film surface exhibited uniaxially aligned nanofibrils oriented along the filament direction (Figure 5C and 5C1). The wall-to-wall crack SEM image exhibited the layered topographical feature of the film which preserved the same fibril orientation from core to surface (Figure 5C and 5C2). Furthermore, birefringent domains are shown to vary in both birefringence intensity and interference color across the width of capillaries and between different capillaries. For all capillary geometries, films were generally more birefringent at the center increasing from the capillary wall. This is consistent with expectation as the solution is subject to varying shear stress from the capillary wall and the mesoscopic structure of the self-assembly was shown to be force responsive. Thus, adjusting capillary geometry and drying

procedure offers further parameters for tuning the mesoscale alignment of peptide film composed by self-assembled nanofibrils.

In conclusion, without using rigid molecular building blocks that are known to facilitate LC formation,[28-31] we designed and synthesized a self-assembling peptide that can carry negative charge by the incorporation of easily protonated functional groups at asymmetric sites to induce a nematic phase. Adjusting the pH level of aqueous environments leads to self-assembling nanofibrils bearing negative charge that align uniaxially in the direction of mechanical force. Via evaporation casting in capillary confinement, solvated self-assembling negatively charged nanofibrils are transformed into highly ordered peptide film as lamellar domains exhibiting various interference colors. The combination of molecular self-assembly into negatively charged fibrils and mechanoresponsive alignment of negatively charged fibrils as a two-step hierarchical regulation is potentially applicable for the fabrication of bio-optic materials,[32] tissue scaffold,[33] and structure-function characterization for the engineering of advanced biomaterials at larger scale.

ASSOCIATED CONTENT

Supporting Information.

The Supporting Information is available free of charge.

Experimental details on molecule synthesis and characterization; Sample preparation protocols; Optical birefringence imaging; TEM imaging and SEM imaging; Optical images of samples; Evaporation casting and imaging (PDF).

AUTHOR INFORMATION

Corresponding Author

*E-mail: ye.zhang@oist.jp

Author Contributions

†These authors contributed equally.

ACKNOWLEDGMENT

The research is supported by Okinawa Institute of Science and Technology Graduate University (OIST), Proof-of-Concept (POC) Program of OIST and Takeda Science Foundation for medical science.

REFERENCES

1. Katoh, K.; Hammar, K.; Smith, P. J. S.; Oldenbourg, R., Birefringence imaging directly reveals architectural dynamics of filamentous actin in living growth cones. *Mol Biol Cell* **1999,** *10* (1), 197-210.

2. Katta, P.; Alessandro, M.; Ramsier, R. D.; Chase, G. G., Continuous electrospinning of aligned polymer nanofibers onto a wire drum collector. *Nano Lett* **2004,** *4* (11), 2215-2218.

3. Pan, H.; Li, L. M.; Hu, L.; Cui, X. J., Continuous aligned polymer fibers produced by a modified electrospinning method. *Polymer* **2006,** *47* (14), 4901-4904.

4. Zhang, S. M.; Greenfield, M. A.; Mata, A.; Palmer, L. C.; Bitton, R.; Mantei, J. R.; Aparicio, C.; de la Cruz, M. O.; Stupp, S. I., A self-assembly pathway to aligned monodomain gels. *Nat Mater* **2010,** *9* (7), 594-601.

5. Cao, H.; Yuan, Q. Z.; Zhu, X. F.; Zhao, Y. P.; Liu, M. H., Hierarchical Self-Assembly of Achiral Amino Acid Derivatives into Dendritic Chiral Nanotwists. *Langmuir* **2012,** *28* (43), 15410-15417.

6. Whitesides, G. M.; Mathias, J. P.; Seto, C. T., Molecular Self-Assembly and Nanochemistry - a Chemical Strategy for the Synthesis of Nanostructures. *Science* **1991,** *254* (5036), 1312-1319.

7. Fredy, J. W.; Mendez-Ardoy, A.; Kwangmettatam, S.; Bochicchio, D.; Matt, B.; Stuart, M. C. A.; Huskens, J.; Katsonis, N.; Pavan, G. M.; Kudernac, T., Molecular photoswitches mediating the strain-driven disassembly of supramolecular tubules. *P Natl Acad Sci USA* **2017,** *114* (45), 11850-11855.

8. Ariga, K.; Ji, Q. M.; Nakanishi, W.; Hill, J. P.; Aono, M., Nanoarchitectonics: a new materials horizon for nanotechnology. *Mater Horiz* **2015,** *2* (4), 406-413.

9. Mendez-Ardoy, A. M.; Granja, J. R.; Montenegro, J., pH-Triggered self-assembly and hydrogelation of cyclic peptide nanotubes confined in water micro-droplets. *Nanoscale Horiz* **2018,** *3* (4), 391-396.

10. Fang, P. A.; Conway, J. F.; Margolis, H. C.; Simmer, J. P.; Beniash, E., Hierarchical self-assembly of amelogenin and the regulation of biomineralization at the nanoscale. *P Natl Acad Sci USA* **2011,** *108* (34), 14097-14102.

11. Du, X. W.; Zhou, J.; Shi, J. F.; Xu, B., Supramolecular Hydrogelators and Hydrogels: From Soft Matter to Molecular Biomaterials. *Chem Rev* **2015,** *115* (24), 13165-13307.

12. Shang, Y.; Zhi, D.; Feng, G.; Wang, Z.; Mao, D.; Guo, S.; Liu, R.; Liu, L.; Zhang, S.; Sun, S.; Wang, K.; Kong, D.; Gao, J.; Yang, Z., Supramolecular Nanofibers with Superior Bioactivity to Insulin-Like Growth Factor-I. *Nano Lett* **2019,** *19* (3), 1560-1569.

13. Zhang, Y.; Kuang, Y.; Gao, Y. A.; Xu, B., Versatile Small-Molecule Motifs for Self-Assembly in Water and the Formation of Biofunctional Supramolecular Hydrogels. *Langmuir* **2011,** *27* (2), 529-537.

14. Tang, J. X.; Janmey, P. A., The polyelectrolyte nature of F-actin and the mechanism of actin bundle formation. *J Biol Chem* **1996,** *271* (15), 8556-8563.

15. Hansen, S. H.; Andersen, M. L.; Cornett, C.; Gradinaru, R.; Grunnet, N., A role for taurine in mitochondrial function. *J Biomed Sci* **2010,** *17* (1), 523.

16. Fatayer, S.; Albrecht, F.; Zhang, Y. L.; Urbonas, D.; Pena, D.; Moll, N.; Gross, L., Molecular structure elucidation with charge-state control. *Science* **2019,** *365* (6449), 142-145.

17. Hall, M. S.; Alisafaei, F.; Ban, E.; Feng, X. Z.; Hui, C. Y.; Shenoy, V. B.; Wu, M. M., Fibrous nonlinear elasticity enables positive mechanical feedback between cells and ECMs. *P Natl Acad Sci USA* **2016,** *113* (49), 14043-14048.

18. Frederix, P. W. J. M.; Ide, J.; Altay, Y.; Schaeffer, G.; Surin, M.; Beljonne, D.; Bondarenko, A. S.; Jansen, T. L. C.; Otto, S.; Marrink, S. J., Structural and Spectroscopic Properties of Assemblies of Self-Replicating Peptide Macrocycles. *Acs Nano* **2017,** *11* (8), 7858-7868.

19. Huang, Z.; Lee, H.; Lee, E.; Kang, S. K.; Nam, J. M.; Lee, M., Responsive nematic gels from the self-assembly of aqueous nanofibres. *Nat Commun* **2011,** *2*.

20. Zhou, J.; Du, X. W.; Gao, Y.; Shi, J. F.; Xu, B., Aromatic-Aromatic Interactions Enhance Interfiber Contacts for Enzymatic Formation of a Spontaneously Aligned Supramolecular Hydrogel. *J Am Chem Soc* **2014,** *136* (8), 2970-2973.

21. Zhao, F.; Gao, Y. A.; Shi, J. F.; Browdy, H. M.; Xu, B., Novel Anisotropic Supramolecular Hydrogel with High Stability over a Wide pH Range. *Langmuir* **2011,** *27* (4), 1510-1512.

22. Le Clainche, C.; Carlier, M. F., Regulation of actin assembly associated with protrusion and adhesion in cell migration. *Physiol Rev* **2008,** *88* (2), 489-513.

23. Gu, Z.; Kothary, P.; Sun, C. H.; Gari, A.; Zhang, Y.; Taylor, C.; Jiang, P., Evaporation-Induced Hierarchical Assembly of Rigid Silicon Nanopillars Fabricated by a Scalable Two-Level Colloidal Lithography Approach. *ACS Appl Mater Interfaces* **2019,** *11* (43), 40461-40469.

24. Insua, I.; Montenegro, J., 1D to 2D Self Assembly of Cyclic Peptides. *J Am Chem Soc* **2020,** *142* (1), 300-307.

25. Paik, T.; Yun, H.; Fleury, B.; Hong, S. H.; Jo, P. S.; Wu, Y. T.; Oh, S. J.; Cargnello, M.; Yang, H.; Murray, C. B.; Kagan, C. R., Hierarchical Materials Design by Pattern Transfer Printing of Self-Assembled Binary Nanocrystal Superlattices. *Nano Lett* **2017,** *17* (3), 1387-1394.

26. Wang, Y. L.; Xia, Y. N., Bottom-up and top-down approaches to the synthesis of monodispersed spherical colloids of low melting-point metals. *Nano Lett* **2004,** *4* (10), 2047-2050.

27. Cherpak, V.; Korolovych, V. F.; Geryak, R.; Turiv, T.; Nepal, D.; Kelly, J.; Bunning, T. J.; Lavrentovich, O. D.; Heller, W. T.; Tsukruk, V. V., Robust Chiral Organization of Cellulose Nanocrystals in Capillary Confinement. *Nano Lett* **2018,** *18* (11), 6770-6777.

28. Kato, T.; Hirai, Y.; Nakaso, S.; Moriyama, M., Liquid-crystalline physical gels. *Chem Soc Rev* **2007,** *36* (12), 1857-1867.

29. Kato, T.; Kutsuna, T.; Yabuuchi, K.; Mizoshita, N., Anisotropic self-aggregation of an anthracene derivative: Formation of liquid-crystalline physical gels in oriented states. *Langmuir* **2002,** *18* (18), 7086-7088.

30. Mizoshita, N.; Hanabusa, K.; Kato, T., Self-aggregation of an amino acid derivative as a route to liquid-crystalline physical gels - Faster response to electric fields. *Adv Mater* **1999,** *11* (5), 392-394.

31. Yabuuchi, K.; Rowan, A. E.; Nolte, R. J. M.; Kato, T., Liquid-crystalline physical gels: Self-aggregation of a gluconamide derivative in mesogenic molecules for the formation of anisotropic functional composites. *Chem Mater* **2000,** *12* (2), 440-443.

32. Tadepalli, S.; Slocik, J. M.; Gupta, M. K.; Naik, R. R.; Singamaneni, S., Bio-Optics and Bio-Inspired Optical Materials. *Chem Rev* **2017,** *117* (20), 12705-12763.

33. Wang, Y. J.; Shang, S. H.; Li, C. Z., Aligned Biomimetic Scaffolds as a New Tendency in Tissue Engineering. *Curr Stem Cell Res T* **2016,** *11* (1), 3-18.